AD-A188 866

(4)

DTNSRDC/SHD-1233-01 FORCES AND MOMENTS ACTING ON A SUBMERSIBLE MOVING BENEATH THE FREE SURFACE OR NEAR A WALL

David W. Taylor Naval Ship Research and Development Center
Bethesda, MD 20084-5000

DTNSRDC/SHD-1233-01 July 1987

Ship Hydrodynamics Department

Submarine Dynamics Branch

FORCES AND MOMENTS ACTING ON A SUBMERSIBLE MOVING BENEATH THE FREE SURFACE OR NEAR A WALL

by

Young S. Hong

APPROVED FOR PUBLIC RELEASE: DISTRIBUTION UNLIMITED

UNCLASSIFIED

SECURITY CLASSIFICATION OF THIS PAGE

REPORT DOCUMENTATION PAGE

1a REPORT SECURITY CLASSIFICATION: UNCLASSIFIED	1b. RESTRICTIVE MARKINGS
2a SECURITY CLASSIFICATION AUTHORITY	3 DISTRIBUTION / AVAILABILITY OF REPORT
2b DECLASSIFICATION / DOWNGRADING SCHEDULE	
4 PERFORMING ORGANIZATION REPORT NUMBER(S): DTNSRDC/SHD-1233-01	5 MONITORING ORGANIZATION REPORT NUMBER(S)
6a NAME OF PERFORMING ORGANIZATION: David W. Taylor Naval Ship Research and Development Center; 6b OFFICE SYMBOL (If applicable): Code 1564	7a. NAME OF MONITORING ORGANIZATION
6c ADDRESS (City, State, and ZIP Code): Bethesda, Maryland 20084	7b ADDRESS (City, State, and ZIP Code)
8a NAME OF FUNDING / SPONSORING ORGANIZATION: Naval Sea Systems Command; 8b OFFICE SYMBOL (If applicable)	9 PROCUREMENT INSTRUMENT IDENTIFICATION NUMBER
8c ADDRESS (City, State, and ZIP Code): Washington, DC 20362	10 SOURCE OF FUNDING NUMBERS: PROGRAM ELEMENT NO; PROJECT NO; TASK NO; WORK UNIT ACCESSION NO

11 TITLE (Include Security Classification)
Forces and Moments Acting on a Submersible Moving Beneath the Free Surface or Near a Wall

12 PERSONAL AUTHOR(S)
Young S. Hong

13a TYPE OF REPORT	13b TIME COVERED	14 DATE OF REPORT (Year, Month, Day)	15 PAGE COUNT
Final	FROM ____ TO ____	1987 July	

16 SUPPLEMENTARY NOTATION

17 COSATI CODES			18 SUBJECT TERMS (Continue on reverse if necessary and identify by block number)
FIELD	GROUP	SUB-GROUP	

19 ABSTRACT (Continue on reverse if necessary and identify by block number)

The forces and moments acting on a submersible are computed when it is beneath the free surface or near a wall. The method used in this report is based on potential theory. In the computation of forces and moments on the hull, a three-dimensional method is applied. The free surface condition is linearized and the body boundary condition is exact. The body surface is discretized with surface elements and the singularity of source and sink is distributed on them. The strengths of the unknown sources and sinks are determined through the body boundary condition. A two-dimensional method is applied to compute forces and moments of the control surfaces. The boundary conditions are same as those for three-dimensional case. Computed forces and moments of the control planes are added to those of the bare hull. To include the interference effect of the hull on the control planes, the flow velocity at each control plane is computed with existence of the hull. There are some discrepancies between computed results and experimental data because of the effect of viscosity. The overall trends in the computed results are same as those of the experiments.

20 DISTRIBUTION / AVAILABILITY OF ABSTRACT: ☒ UNCLASSIFIED/UNLIMITED ☐ SAME AS RPT ☐ DTIC USERS	21 ABSTRACT SECURITY CLASSIFICATION
22a NAME OF RESPONSIBLE INDIVIDUAL: Young S. Hong	22b TELEPHONE (Include Area Code): 202-227-1080; 22c OFFICE SYMBOL: Code 1564

DD FORM 1473, 84 MAR — 83 APR edition may be used until exhausted. All other editions are obsolete

SECURITY CLASSIFICATION OF THIS PAGE

UNCLASSIFIED

CONTENTS

FIGURES

NOTATION

C	Chord of control plane section
$C_L = \dfrac{F_z}{\frac{\rho}{2} U^2 C}$	Lift coefficient of control plane section
D	Diameter of the submerged body
E_1	Exponential Integral
F_x	Axial Force
F_z	Vertical force
$F_x' = \dfrac{F_x}{\frac{\rho}{2} U^2 L^2}$	Non-dimensionalized axial force
$F_z' = \dfrac{F_z}{\frac{\rho}{2} U^2 L^2}$	Non-dimensionalized vertical force
$F_n = \dfrac{U}{\sqrt{gL}}$	Froude number of the submersible
$F_c = \dfrac{U}{\sqrt{gC}}$	Froude number of the control plane section
g	Gravitational acceleration
G	Three-dimensional Green function
G_2	Two-dimensional Green function
h	Depth to the axis of revolution of the submerged body
h_1	Depth of submergence to control plane section at quarter chord
h_2	Depth of submergence to control plane section at mid chord
$i = \sqrt{(-1)}$	Imaginary Unit
L	Length of the submersible
M_y	Moment about the oy-axis

$M_y' = \frac{M_y}{\frac{\rho}{2} U^2 L^3}$ Non-dimensionalized moment about the oy-axis

$\vec{n}$ Unit vector of the body surface drawn into the fluid

p Pressure

[illegible] Position vector of the center of gravity

U Speed

ρ Water density

α Angle of attack of the control plane section

θ Pitch angle of the bare hull

Γ Vortex strength

σ Source or sink strength

Φ Three-dimensional velocity potential

ϕ Two-dimensional velocity potential

ABSTRACT

The forces and moments acting on a submersible are computed when it is beneath the free surface or near a wall. The method used in this report is based on potential theory. In the computation of forces and moments on the hull, a three-dimensional method is applied. The free surface condition is linearized and the body boundary condition is exact. The body surface is discretized with surface elements and the singularity of source and sink is distributed on them. The strengths of the unkown sources and sinks are determined through the body boundary condition. A two-dimensional method is applied to compute forces and moments of the control surfaces. The boundary conditions are same as those for three-dimensional case. Computed forces and moments of the control planes are added to those of the bare hull. To include the interference effect of the hull on the control planes, the flow velocity at each control plane is computed with existence of the hull. There are some discrepancies between computed results and experimental data because of the effect of viscosity. The overall trends in the computed results are same as those of the experiments.

ADMINISTRATIVE INFORMATION

The work described below was performed for the Naval Sea System Command (NAVSEA). Funding was provided under Work Unit Number 1563-172.

INTRODUCTION

There is a need to develop an analytical method to compute the forces and moments acting on a submersible when it is beneath the free surface or near a wall. The methodologies presently available to compute these hydrodynamic forces and moments are limited in application. Pond[1]* computed the moments developed on a Rankine ovoid by using the method of axial distribution of sources and sinks. McCreight[2] improved the method used by Pond by distributing the dipoles and computed the vertical force. Their results are in good agreement with the experimental data. However, the methods used by Pond and McCreight are valid only for zero pitch angle.

The present method computes the vertical and longitudinal forces and pitch moment acting on a submersible with and without control planes when the submersible moves beneath the free surface or near a wall. This method is more accurate mathematically than that of Pond[1]. Furthermore, the effect of pitch angle is incorporated in the computation. For the computation of forces and moment acting on the bare hull, the so-called panel method is applied. The body surface is discretized with many quadrilateral planes, and sources and sinks are distributed on these surface elements. This method can be applied to a submerged body of arbitrary shape. To compute the forces and moment of the control planes, the method developed by Giesing and Smith[3] is used. Two-dimensional sources and sinks are distributed around the sections of a control plane, and a vortex located in the middle of each section is introduced to compute lift force. The inlet velocity to the control planes is computed at the tips of the sections of the control plane to include the interaction effort between the bare hull and control planes.

*References are given on page 45.

VELOCITY POTENTIAL

HULL

The coordinate system, oxyz, moves at a speed U, which is the mean forward speed of the submersible along the positive ox-axis (see Figure 1). The positive oz-axis is always directed vertically upwards. The origin 0 is located above the center of gravity of the submersible. The oxy-plane is the plane of the undisturbed free surface.

We assume initially that the submersible and coordinate system are stationary and that the fluid around the submersible moves toward the negative ox-axis with uniform speed U. Then, the total velocity potential for the bare hull can be expressed by

$$\Phi(x,y,z) = -Ux + \phi(x,y,z) \tag{1}$$

where ϕ is disturbance velocity potential due to the submersible. The disturbance velocity potential satisfies the following conditions:

1. Laplace equation in the fluid domain

$$\frac{\partial^2 \phi}{\partial x^2} + \frac{\partial^2 \phi}{\partial y^2} + \frac{\partial^2 \phi}{\partial z^2} = 0 \tag{2}$$

2. The linearized free-surface condition

$$\frac{\partial^2 \phi}{\partial x^2} + k_o \frac{\partial \phi}{\partial z} = 0 \tag{3}$$

3. The body boundary condition

$$\frac{\partial \phi}{\partial n} = U\, n_1 \tag{4}$$

4. The radiation condition: the disturbance vanishes sufficiently fast far ahead of the ship.

$$\lim_{x \to \infty} \bar{R}(\phi_x^2 + \phi_y^2 + \phi_z^2) = 0 \tag{5}$$

$$\bar{R} = (x^2 + y^2)^{1/2}$$

5. The bottom condition: the normal velocity at the bottom is zero.

$$\phi_z(x,y,z) = 0 \quad \text{as } z \to -\infty \tag{6}$$

In equation (3), the constant is given as

$$k_o = \frac{g}{U^2} \tag{7}$$

and in Equation (4), the unit vector which is oriented normal to the fluid is given by

$$\begin{aligned} (n_1, n_2, n_3) &= \vec{n} \\ (n_4, n_5, n_6) &= \vec{r}_G \times \vec{n} \end{aligned} \tag{8}$$

where $\vec{r}_G$ is the position vector of the center of gravity.

The solution of Equation (2) is given by Brard[4] in an integral form as

$$\phi(x,y,z) = -\frac{1}{4\pi} \iint_S G(P,Q)\sigma(Q)dS(Q) \tag{9}$$

where $P(x,y,z)$ is the field point, $Q(x_o,y_o,z_o)$ the source point, S the wetted surface of the body, σ the unknown strength of sources and sinks distributed on the body surface, and G is the Green function which is given by Wehausen and Laitone[5] as

$$G(P,Q) = \frac{1}{r} - \frac{1}{r_1} - \frac{k_o}{\pi} \int_{-\pi}^{\pi} \sec^2\theta \, d\theta \int_0^\infty \frac{e^{-(z+z_o)u} e^{i\tilde{\omega}u}}{u - k_o \sec^2\theta} \, du \tag{10}$$

where

$$r^2 = (x - x_o)^2 + (y - y_o)^2 + (z - z_o)^2 \tag{11}$$

$$r_1^2 = (x - x_o)^2 + (y - y_o)^2 + (z + z_o)^2 \tag{12}$$

and

$$\tilde{\omega} = (x - x_o)\cos\theta + (y - y_o)\sin\theta \tag{13}$$

Only the real part of Equation (10) is used in later computation.

The strength of the sources and sinks, σ, in Equation (9) can be found by substitution of Equation (9) into Equation (4) to obtain

$$\frac{1}{4\pi} \frac{\partial}{\partial n} \iint_S G(P,Q)\sigma(Q)ds(Q) = -Un_1 \tag{14}$$

The solution of Equation (14) is only feasible with the help of a numerical procedure which will be given later.

The force acting on the body is expressed as

$$\vec{F} = -\iint_S p \, \vec{n} \, ds \tag{15}$$

where p is the pressure around the body and is linearized from Bernoulli's equation as

$$p = \rho U \phi_x \tag{16}$$

where ρ is the density of the fluid.

CONTROL PLANE

The velocity potential for the control plane, whose coordinate system is shown in Figure 2, is expressed in the two-dimensional domain as

$$\Phi(x,z) = -Ux + \phi(x,z) \tag{17}$$

where ϕ is the disturbance velocity potential due to a section of the control plane. This disturbance potential satisfies the following conditions.

1. Laplace equation in the fluid domain

$$\frac{\partial^2 \phi}{\partial x^2} + \frac{\partial^2 \phi}{\partial z^2} = 0 \tag{18}$$

2. The linearized free-surface condition

$$\frac{\partial^2 \phi}{\partial x^2} + k_o \frac{\partial \phi}{\partial z} = 0 \tag{19}$$

3. The body boundary condition

$$\frac{\partial \phi}{\partial n} = Un_1 \tag{20}$$

4. Kutta condition: the velocities at the trailing edge elements, one at the top of the surface and one at the bottom, are equal.

In addition, the disturbance potential should satisfy radiation and bottom conditions similar to Equations (5) and (6).

The solution of Equation (18) is given by Giesing and Smith[3]. The velocity potential function is divided into three parts as

$$\phi(x,z) = \phi_1 + \Gamma(\phi_2 + \phi_3). \tag{21}$$

The velocity potential ϕ_1 is due to sources and sinks which are distributed on each section of the control plane. ϕ_2 is the velocity potential due to a vortex of unit strength which is located at the inside of a section. The vortex is introduced to calculate the lift force around the section. ϕ_3, the last term of Equation (21) is the velocity potential due to sources and sinks of unit strength distributed on the section. This velocity potential cancels the normal velocity generated by ϕ_2. If we substitute Equation (21) into Equation (20), the following conditions are given

$$\frac{\partial \phi_1}{\partial n} = Un_1 \tag{22}$$

and

$$\frac{\partial \phi_2}{\partial n} = - \frac{\partial \phi_3}{\partial n} \quad . \tag{23}$$

These three velocity potentials are expressed as

$$\phi_i(P) = \frac{1}{2\pi} \int_C \sigma_i(q) G_2(p,q) dl(q) \quad \text{for } i=1 \text{ and } 3 \tag{24}$$

and

$$\phi_2(P) = \mathrm{Re}\Big\{ \frac{i}{2\pi} \ln\left[x-a + i(z-b)\right] - \frac{i}{2\pi} \ln\left[(x-a) + i(z+b)\right]$$

$$-2pv \int_0^\infty \frac{e^{-ik[x-a + i(z+b)]}}{k - k_o} dk + 2\pi i\, e^{-ik_o[x-a + i(z+b)]} \Big\}$$

where σ_i is the two-dimensional strength of sources and sinks, (a,b) the location of the vortex, $q(x_o,z_o)$ a two-dimensional source point, and G_2 is the two-dimensional Green function given by Wehausen and Laitone[5] as

$$G_2(p,q) = \text{Re}\ \Big\{\ln\ [x-x_o + i(z-z_o)] + \ln[x-x_o + i(z+z_o)]$$

$$+ 2\text{pv} \int_0^\infty \frac{e^{-ik[x-x_o + i(z+z_o)]}}{k - k_o}\, dk - 2\pi i\ e^{-ik_o[x-x_o + i(z+z_o)]}\Big\} \tag{26}$$

In Equations (25) and (26), Re denotes the real part of a complex quantity and pv the principal-value integral. The vortex strength Γ in Equation (21) will be determined with the Kutta condition. The pressure around each section of the control plane can be obtained from Equation (16) by substituting Φ_x for ϕ_x. The force and moment acting on the section can be computed with an equation of the same form as Equation (15).

By substituting Equation (24) into either Equation (22) or Equation (23), the unknown strength of the sources and sinks for the two-dimensional case can be determined from the following equation

$$\frac{1}{2\pi}\frac{\partial}{\partial n}\int_C \sigma_i(q)G_2(p,q)dl(q) = Un_i \quad \text{for } i = 1 \tag{27}$$

$$= -\frac{\partial \Psi_3}{\partial n} \text{ for } i=3.$$

When the submersible is moving near a wall, the linear free-surface conditions, Equations (3) and (19) are no longer valid. Instead, we should use the wall boundary conditions given by

$$\frac{\partial \phi}{\partial z} = 0 \qquad \text{at } z = 0 \tag{28}$$

and

$$\frac{\partial \phi}{\partial z} = 0 \qquad \text{at } z = 0 \tag{29}$$

All other boundary conditions are the same as those described in Equations (2), (4) - (6), (18) and (20). The solutions in this case have the same form as Equations (9) and (21), with different Green functions. The Green functions can be expressed by application of the method of images (see Reference 6) as

$$G(P,Q) = \frac{1}{r} + \frac{1}{r_1} \tag{30}$$

for the case of bare hull and

$$G_2(p,q) = \mathrm{Re}\{\ln[x-x_0 + i(z-z_0)] + \ln[x-x_0 + i(z+z_0)]\} \tag{31}$$

for the case of control plane. The velocity potential due to a unit vortex located at (a,b) should be

$$\phi_2(p) = \mathrm{Re}\{\frac{i}{2\pi} \ln[(x-a) + i(z-b)] - \frac{i}{2\pi} \ln[(x-a) + i(z+b)]\} \tag{32}$$

To find the velocity potentials for the wall condition, Equations (10), (25) and (26) should be replaced by Equations (30), (32) and (31), respectively.

NUMERICAL PROCEDURE

To determine the unknown strength of the sources and sinks in Equation (14), we first discretize the wetted surface of the body S with many quadrilateral elements. Figure 3 shows the discretized surfaces of a spheroid. Furthermore, we assume that the unknown strength of the sources and sinks, $\sigma(Q)$, is constant on each surface element. Then Equation (14) can be written as follows

$$\frac{1}{4\pi} \sum_{j=1}^{N} \sigma_j(Q_j) \frac{\partial}{\partial n} G(P_i,Q_j) \, \Delta S_j = -Un_{1i} \qquad \text{for } i = 1, 2, \ldots, N \tag{33}$$

Once the derivations of the Green function, G, are evaluated numerically, Equation (33) can easily be solved for σ_j. The numerical evaluation of the Green function and its derivatives is the most difficult part, and consumes a lot of computer time when running the program.

The normal derivative of the Green function in Equation (33) can be expressed as

$$\frac{\partial G}{\partial n} = \frac{\partial G}{\partial x} n_1 + \frac{\partial G}{\partial y} n_2 + \frac{\partial G}{\partial z} n_3 \quad . \tag{34}$$

The task is to find three derivatives of the Green function. To do this, we first derive the Green function suitable to numerical evaluation. The Green function, Equation (10), can be rewritten as

$$G = \frac{1}{r} - \frac{1}{r_1} - \frac{k_o}{\pi} \int_0^{\frac{\pi}{2}} \sec^2\theta \, d\theta \, \Big\{ \underset{(L_1)}{\int_0^\infty} \frac{e^{-\bar{z}u}(e^{i\tilde{\omega}_+ u} + e^{i\tilde{\omega}_- u})}{u - u_o} \, du$$

$$+ \underset{(L_2)}{\int_0^\infty} \frac{e^{-\bar{z}u}(e^{-i\tilde{\omega}_+ u} + e^{-i\tilde{\omega}_- u})}{u - u_o} \, du \Big\} \tag{35}$$

where

$$\tilde{\omega}_+ = (x-x_o) \cos \theta + (y-y_o) \sin \theta = \tilde{\omega}$$

$$\tilde{\omega}_- = (x-x_o) \cos \theta - (y-y_o) \sin \theta \tag{36}$$

$$\bar{z} = |z + z_o|$$

$$u_o = k_o \sec^2\theta$$

The notation under two of the integrals in Equation (35), namely, L_1 or L_2, represents the integral paths shown in Figure 4. To derive the derivatives of the first two terms of Equation (35), the method which Hess and Smith[7] developed for unbounded flow can be used. Hong and Paulling[8] have applied this method for the computation of motions of a body in waves, and their paper can be examined for the details. Since Reference 8 can be examined for these details, we will present here the derivation of the last two terms of Equation (35).

We write Equation (35) as follows

$$G = \frac{1}{r} - \frac{1}{r_1} + G_3 \tag{37}$$

$$G_3 = -\frac{1}{\pi} \int_o^{\frac{\pi}{2}} u_o \, d\theta \left\{ \int_{\substack{o \\ (L_1)}}^{\infty} \frac{e^{-\bar{z}u}(e^{i\tilde{\omega}_+ u} + e^{i\tilde{\omega}_- u})}{u - u_o} du + \int_{\substack{o \\ (L_2)}}^{\infty} \frac{e^{-\bar{z}u}(e^{-i\tilde{\omega}_+ u} + e^{i\tilde{\omega}_- u})}{u - u_o} du \right\} \tag{38}$$

We now change the variable for the integral path, L_1, as follows:

$$v = (u-u_o)(\bar{z}-i\tilde{\omega}) \qquad \text{with } \tilde{\omega} = \tilde{\omega}_+ \text{ or } \tilde{\omega}_-;$$

then, the integral path becomes that shown in Figure 5. The integral path, L_1, is now transferred onto the path C, in Figure 5 as

$$\int_{\substack{0 \\ (L_1)}}^{\infty} \frac{e^{-\bar{z}u}\, e^{i\tilde{\omega}_- u}}{u - u_o}\, du = e^{-u_o(\bar{z} - i\tilde{\omega})} \int_{C_1} \frac{e^{-v}}{v}\, dv \tag{39}$$

The integral over C_1 can be easily evaluated with the method of residue as

$$\int_{C_1} \frac{e^{-v}}{v}\, dv = \int_{u_o(z - i\tilde{\omega})}^{\infty} \frac{e^{-v}}{v}\, dv + \left\{ \begin{matrix} -2\pi i \\ 0 \end{matrix} \right\}, \quad \begin{matrix} \tilde{\omega} < o \\ \tilde{\omega} > o \end{matrix} \tag{40}$$

with the introduction of the exponential integral

$$\int_{-u_o(z - i\tilde{\omega})}^{\infty} \frac{e^{-v}}{v}\, dv = E_1[-u_o(z - i\tilde{\omega})], \tag{41}$$

the integral over C_1 becomes

$$\int_{C_1} \frac{e^{-v}}{v}\, dv = E_1[-u_o(\bar{z} - i\tilde{\omega})] + \left\{ \begin{matrix} -2\pi i \\ 0 \end{matrix} \right\}, \quad \begin{matrix} \tilde{\omega} < o \\ \tilde{\omega} > o \end{matrix} \tag{42}$$

By substituting Equation (37) into Equation (33), the integral over L_1 is given by

$$\int_{\substack{o \\ (L_1)}} \frac{e^{-\bar{z}u}(e^{i\tilde{\omega}_+ u} + e^{i\tilde{\omega}_- u})}{u - u_o}\, du = e^{-u_o(\bar{z} - i\tilde{\omega}_+)} \left\{E_1\left[-u_o(\bar{z} - i\tilde{\omega}_+)\right] - {2\pi i \atop 0}\right\}$$

$$+ e^{-u_o(\bar{z} - i\tilde{\omega}_-)} \left\{E_1\left[-u_o(\bar{z} - i\tilde{\omega}_-)\right] + \left\{{2\pi i \atop 0}\right\}, \quad {\tilde{\omega}_+, \tilde{\omega}_- < o \atop \tilde{\omega}_+, \tilde{\omega}_- > o}\right. \tag{43}$$

For the integral path, L_2, we change the variable as follows:

$$v = (u - u_o)\ (\bar{z} + i\tilde{\omega}) \qquad \text{with} \qquad \tilde{\omega} = \tilde{\omega}_+ \text{ or } \tilde{\omega}_-;$$

then, the new integral path is given in Figure 6. With this new variable, the integral path, L_2, is now C_1. Employing the same procedure as used previously to evaluate the integral over L_1, the integral over L_2 becomes

$$\int_{\substack{o \\ (L_2)}}^{\infty} \frac{e^{-\bar{z}u}(e^{i\tilde{\omega}_+ u} + e^{-i\tilde{\omega}_- u})}{u - u_o}\, du = e^{u_o(\bar{z} + i\tilde{\omega}_+)} \left\{E_1\left[-u_o(\bar{z} + i\tilde{\omega}_+)\right] + {2\pi i \atop 0}\right\}$$

$$+ \ e^{-u_o(\bar{z} + i\tilde{\omega}_-)}\left\{E_1\left[-u_o(\bar{z} + i\tilde{\omega}_-)\right] + {2\pi i \atop 0}\right\}, \quad {\tilde{\omega}_+, \tilde{\omega}_- < o \atop \tilde{\omega}_+, \tilde{\omega}_- > o} \tag{44}$$

Substitution of Equation (43) and (44) into Equation (38), allows us finally to express G_3 in a convenient form for numerical evaluation as

$$
\begin{aligned}
G_3 = -\frac{1}{\pi}\int_0^{\pi/2} u_o \, d\theta \, \Big\{ & e^{-u_o(\bar{z} - i\tilde{\omega}_+)} \Big\{E_1\left[-u_o(\bar{z} - i\tilde{\omega}_+)\right] - \substack{2\pi i \\ 0}\Big\} \\
& + e^{-u_o(\bar{z} - i\tilde{\omega}_-)} \Big\{E_1\left[u_o(\bar{z} - i\tilde{\omega}_-)\right] - \substack{2\pi i \\ 0}\Big\} \\
& + e^{-u_o(\bar{z} + i\tilde{\omega}_+)} \Big\{E_1\left[-u_o(\bar{z} + i\tilde{\omega}_+)\right] + \substack{2\pi i \\ 0}\Big\} \\
& + e^{-u_o(\bar{z} + i\tilde{\omega}_-)} \Big\{E_1\left[-u_o(\bar{z} + i\tilde{\omega}_-)\right] + \substack{2\pi i \\ 0}\Big\}\Big\}, \quad \begin{matrix} \tilde{\omega}_+, \ \tilde{\omega}_- < 0 \\ \tilde{\omega}_+, \ \tilde{\omega}_- > 0 \end{matrix}
\end{aligned}
\tag{45}
$$

If we let

$$
\begin{aligned}
& u_0 e^{-u_o(\bar{z} - i\tilde{\omega}_+)} \, E_1\left[-u_o(\bar{z} - i\tilde{\omega}_+)\right] = R + iI \\
& u_0 e^{-u_o(\bar{z} - i\tilde{\omega}_+)} = C + iS \\
& u_0 e^{-u_o(\bar{z} - i\tilde{\omega}_-)} \, E_1\left[u_o(\bar{z} - i\tilde{\omega}_-)\right] = \bar{R} + i\bar{I} \\
& u_0 e^{-u_o(\bar{z} - i\tilde{\omega}_-)} = \bar{C} + i\bar{S}
\end{aligned}
\tag{46}
$$

we can express G_3 as

$$G_3 = -\frac{2}{\pi}\int_0^{\pi/2}\left[R^+\binom{2\pi}{0}S^+ + R^-\binom{2\pi}{0}S^-\right]d\bar{\theta}, \quad \begin{array}{l}\omega_+, \tilde{\omega}_- \lessgtr 0 \\ \tilde{\omega}_+, \tilde{\omega}_- > 0\end{array} \tag{47}$$

The derivatives of G_3 can be easily expressed from Equation (38)

$$\frac{\partial G_3}{\partial x} = i\ u \cos\theta\ G_3 \tag{48}$$

$$\frac{\partial G_3}{\partial y} = i\ u \sin\theta\ G_3\ \mathrm{sign}(\tilde{\omega}) \tag{49}$$

$$\frac{\partial G3}{\partial z} = u\ G_3 \tag{50}$$

where

$$\begin{aligned}\mathrm{sign}\ (\tilde{\omega}) &= 1 \quad \text{for} \quad \tilde{\omega} = \tilde{\omega}_+ \\ &= -1 \qquad\quad \tilde{\omega} = \tilde{\omega}_-\end{aligned} \tag{51}$$

With substitution of Equation (45) into Equations (48), (49) and (50), the derivatives of G_3 can be expressed in final form as

$$\frac{\partial G_3}{\partial x} = -\frac{2}{\pi}\int_0^{\pi/2} u_o \cos\theta \; \Big\{ -\frac{\tilde{\omega}_+}{\bar{z}_+^2 + \tilde{\omega}_+^2} - I + \left({}^{2\pi}_{0}\right) C$$

$$+ \frac{\tilde{\omega}_-}{\bar{z}_+^2 + \tilde{\omega}_-^2} - \bar{I} + \left({}^{2\pi}_{0}\right) \bar{C} \Big\} d\theta \qquad (52)$$

$$\frac{\partial G_3}{\partial y} = -\frac{2}{\pi}\int_0^{\pi/2} u_o \sin\theta \; \Big\{ -\frac{\tilde{\omega}_+}{\bar{z}_+^2 + \tilde{\omega}_+^2} - I + \left({}^{2\pi}_{0}\right) C$$

$$+ \frac{\tilde{\omega}_-}{\bar{z}_+^2 + \tilde{\omega}_-^2} + \bar{I} - \left({}^{2\pi}_{0}\right) \bar{C} \Big\} d\theta \qquad (53)$$

$$\frac{\partial G_3}{\partial z} = -\frac{2}{\pi}\int_0^{\pi/2} u_o \; \Big\{ \frac{\bar{z}}{\bar{z}_+^2 + \tilde{\omega}_+^2} + R + \left({}^{2\pi}_{0}\right) S$$

$$+ \frac{\bar{z}}{\bar{z}_+^2 + \tilde{\omega}_-^2} + \bar{R} + \left({}^{2\pi}_{0}\right) \bar{S} \Big\} d\theta \qquad (54)$$

In these equations, the upper value is taken when $\tilde{\omega}_+$ or $\tilde{\omega}_-$ is larger than and equal to 0 and the lower value is taken when $\tilde{\omega}_+$ or $\tilde{\omega}_-$ is negative. Inglis and Price[9] have derived the Green function for a translating and pulsating source similar to G_3 with the change of variable and with the change of integral path.

When the argument, $-u_0(\bar{z}+i\tilde{\omega})$ or $-u_0(\bar{z}-i\tilde{\omega})$ is small, the exponential integral can be expressed in a series form (see Reference 10) as

$$E_1(z) = -\gamma - \ln z - \sum_{n=1}^{\infty} \frac{(-1)^n z^n}{nn!}, \qquad |\arg z| < \pi \tag{55}$$

where z is any complex number and $\gamma = 0.5772157$ is Euler's constant. When the argument becomes very large, the exponential integral is evaluated by the method of Todd.[11] For a large complex number $z = x + iy$, the exponential integral multiplied with exponential funct'on is expressed as

$$e^z E_1(z) = I_1 - iI_2 \tag{56}$$

where

$$I_1 = \int_0^{\infty} e^{-u} \frac{x + u}{(x + u)^2 + y^2} du \tag{57}$$

$$I_2 = \int_0^{\infty} e^{-u} \frac{y}{(x + u)^2 + y^2} du \tag{58}$$

For the evaluation of I_1 and I_2, we use the following approximation

$$I = \int_0^\infty e^{-t} f(t)\, dt \cong \sum \lambda_i^{(n)} f(x_i^{(n)}) \tag{59}$$

where $x_i^{(n)}$ are the zeros of the Laguerre polynomial and $\lambda_i^{(n)}$ are the corresponding Christoffel numbers. In this report, n is taken as 5, and $x_i^{(5)}$ and $\lambda_i^{(5)}$ are given in Table I.

Table I:
Zeros of Laguerre Polynomials and
Christoffel Numbers

$x_i^{(5)}$	$\lambda_i^{(5)}$
0.2635603	0.5217556
1.4134031	1.3986668
3.5964258	0.0759424
7.0858100	0.0036117
12.6408008	0.0000234

The exponential functions in Equations (47), (52), (53) and (54) are highly oscillatory when the real part of the complex argument is small and the imaginary part is large. One of complex arguments in Equation (46) can be expressed as

$$-u_o(\bar{z} - i\tilde{\omega}_+) = -k_o \sec^2\theta \cdot \left[\bar{z} + iR\cos(\theta + \beta)\right] \tag{60}$$

with

$$R^2 = (x - x_o)^2 + (y - y_o)^2$$

$$\beta = \tan^{-1} (\frac{y - y_o}{x - x_o})$$

When $\theta_2 - \theta_1$ is small, the integral between θ_1 and θ_2 can be approximated as

$$\int_{\theta_1}^{\theta_2} u_o(C + iS)d\theta = \int_{\theta_1}^{\theta_2} k_o \sec^2\theta \cdot \exp\{-k_o \sec^2\theta[\overline{z} + iR \cos(\theta + \beta)]\} \tag{61}$$

$$= \int_{\theta_1}^{\theta_2} (A + iB) \exp[i(a\theta + b)]d\theta$$

where A, B, a, and b are constant between θ_1 and θ_2. The last expression in Equation (61) can be analytically evaluated. Once the normal derivative of the Green function, which contains Equation (61), is numerically evaluated, Equation (33) can be expressed as a system of linear equations and σ_j can be solved by the method of Gauss elimination.

For the computation of forces and moment of a control plane, we discretize each section of the control plane with straight segments as shown in Figure 7. The unknown strength of the two-dimensional sources and sinks on each segment is assumed to be constant. The subscript i for σ_i in Equation (27) will be dropped from now on to avoid confusion associated with that of segments. σ represents each of σ_1 and σ_3 in the following equations. Equation (27) can be approximated as

$$\frac{1}{2\pi} \sum_{j=1}^{M} \sigma(q_j) \int_{S_j} \frac{\partial}{\partial n} G_2 (p_i, q_j)\, dS_j(q_j) = U\, n_{1_i}, \quad \text{for } i = 1,2,\ldots,M \tag{62}$$

the normal derivative of the two-dimensional Green function is

$$\frac{\partial G_2}{\partial n} = \frac{\partial G_2}{\partial x} n_1 + \frac{\partial G_2}{\partial z} n_3 \tag{63}$$

We use the complex variables in derivation of derivatives of the Green function suitable for numerical evaluation. If we introduce the following complex variables

$$C = x + iz \qquad \text{and} \qquad C_o = x_o + iz_o, \tag{64}$$

$$G_2(p,q) = \mathrm{Re}\{F(C,C_o)\} \tag{65}$$

where

$$F(C,C_o) = \ln(C - C_o) + \ln(C - \overline{C}_o) + \mathrm{pv} \int_0^\infty \frac{e^{-ik(C - \overline{C}_o)}}{k - k_o}\, dk \tag{66}$$

$$- 2\pi i\, e^{-ik_o(C - \overline{C}_o)}$$

In Equation (66), $\overline{C}_o$ is the complex conjugate of C_o. Then, the two derivatives in Equation (63) can be expressed as functions of F

$$\frac{\partial G_2}{\partial x} = \mathrm{Re}\left\{\frac{\partial F}{\partial C}\right\} \tag{67}$$

and

$$\frac{\partial G_2}{\partial z} = - I_m\left\{\frac{\partial F}{\partial C}\right\} \tag{68}$$

The derivative of Equation (66) with respect to C is

$$\frac{\partial F}{\partial C} = \frac{1}{C - \overline{C}o} + \frac{1}{C - Co} - \frac{i}{\pi} \, pv \int_0^\infty \frac{k \, e^{-ik(C - \overline{C}_o)}}{k - k_o} dk \tag{69}$$

$$- 2\pi \, k_o \, e^{-i \, k_o(C - \overline{C}_o)}$$

Integrating the last equation with respect to $s_j(q_j)$ we obtain

$$\int_{S_j} \frac{\partial F}{\partial C} ds_j(q_j) = -(\cos \alpha_j - i \sin \alpha_j)[\ln r_{j+1} + i\theta_{j+1} - \ln r_j - i\theta_j]$$

$$- (\cos \alpha_j + i \sin \alpha_j)[\ln \overline{r}_{j+1} + i\overline{\theta}_{j+1} - \ln \overline{r}_j - i\overline{\theta}_j]$$

$$- \frac{i}{\pi} (\cos \theta_j + i \sin \alpha_j)\{pv \int_0^\infty \frac{dk}{k - k_o} e^{k(z + z_{o_{j+1}})} [\cos k(x - x_{o_{j+1}})$$

$$- i \sin k(x - x_{o_{j+1}})] - pv \int_0^\infty \frac{dk}{k - k_o} e^{k(z + z_{o_j})} [\cos k(x - x_{o_j})$$

$$- i \sin k(x - x_{o_j})]\}$$

$$+ 2\pi i (\cos \alpha_j + i \sin \alpha_j)\{e^{k_o(z + z_{o_{j+1}})}[\cos k_o(x - x_{o_{j+1}})$$

$$- i \sin k_o(x - x_{o_{j+1}})]$$

$$- e^{k_o(z + z_{o_{j+1}})}[\cos k_o(x - x_{o_j}) - i \sin k_o(x - x_{o_j})]\} \quad (70)$$

the new variable and notation are given in Figure 8. The details for derivation of Equation (70) are given by References 3 and 12.

The numerical procedure for determining σ_1 and Γ is as follows: First, we evaluate the normal derivative of the two-dimensional Green function which enables us to solve Equation (62) for σ_1. Next, we calculate the normal velocities at segments due to a unit vortex located at the center of the section. To eliminate these normal velocities, we distribute σ_3 at each segment of the section and determine σ_3 with Equation (23). We finally solve for the vortex strength Γ in Equation (21) using the Kutta condition.

The computational procedure of forces and moments is as follows: The forces and moments of the bare hull are first computed. This means it is assumed no interference of control planes to the bare hull. To include the interference effect of the bare hull to the control planes, the flow velocity, U, in Figure 2 is different from U in Figure 1. A control plane is cut at three different spanwise locations. At the leading edge of each location (or section), U is computed. This velocity is different from the steady forward speed, U, in Figure 1. Two-dimensional forces and moments are computed at each section; and these are summed along the spanwise direction. Finally, these summed forces and moments are added to those of the bare hull.

NUMERICAL RESULTS

In this section we will calculate the forces and moments acting on a submersible moving under the free surface or under ice. Numerical results based on the present method will be compared with results obtained from earlier theoretical methods and experiments. First, forces acting independently on the bare hull and control plane will be compared; then, results for the combined hull and plane will be compared.

Figure 9 shows the forces and moments on a Rankine ovoid having a length of 4 ft (1.22m). The ratio of length to diameter (D) is 10.5. The Rankine ovoid is created by distributing sources and sinks along a line which is assumed to be in a uniform stream in an unbounded fluid (see Reference 12). The computed vertical forces (F'_z) are generally somewhat larger than the experimental data for smaller submergence (h) and smaller for larger submergence. The computed moments (M'_y) are generally smaller than the experimental data for all submergences when the Froude number is larger than 0.5. However, the overall trend of the computed results is similar to that of the measurements. Results calculated by the present method are in good agreement with values obtained from previous analytical methods. Figure 10 shows the same results plotted as a function of submergence. As the submergence becomes larger than three times the diameter, the force and moments decrease rapidly for all Froude numbers.

Figures 11, 12 and 13 show similar data for a spheroid whose ratio of length to diameter is 7. The findings here are somewhat different from those discussed previously for the Rankine ovoid (see Figure 9). When pitch angle is zero (see Figure 11) the experimental data for the spheroid extracted from Reference 13 are larger than the computed values at Froude numbers less than 0.5. The agreement between computation and experiment is generally good when the submergence is equal to or larger than the diameter: when the ratio of submergence to diameter is 0.75, there is substantial difference. When the pitch angle is 2.5 degrees (bow up), the experimental results are larger than those from computation for essentially all Froude numbers (see Figure 12). As shown in Figure 13, negative pitch angle of 2.5 degrees (bow down), the prediction and measurement of vertical force are, for the most part, in better agreement than those for zero or positive pitch angle. The computed moments are larger than the experimental results for all submergences and Froude numbers. These discrepancies for non-zero pitch angle might be caused by the viscosity of the fluid and also vortex shedding from the body or the cross flow effect.

Figure 14 shows the results of lift for a hydrofoil whose section has the shape of NACA 4412. The results shown in this figure are those for a two-dimensional section. The agreement between computation based on the present method and experimental data from Reference 14 is good when the angle of attack is smaller than 4 degrees (see bottom figure). As the angle of attack increases, the computed results become larger than the measurements particularly at the lower Froude number. It is of interest to observe that for this submergence the lift coefficient at the higher Froude number is smaller than that at the lower Froude number. When the angle of attack is 10 degrees and the Froude number is 0.922 (see top figure) there is substantial discrepancy between the computed and experimental results as the submergence increases. The results computed by the present method are further compared with the method developed by Wadlin and Christopher in Reference 17, Equation (15). The calculations were made for an aspect ratio of 10 to stimulate a two-dimensional lift coefficient. It should be pointed out that Equation (15) of Reference 17 is strictly applicable for aspect ratio of 0.125 to 10. Their results are almost half of those by the present method. Compared with the experiment, the results of Wadlin and Christopher show better agreement than those by the present method.

Figure 15 shows the results of lift for a hydrofoil whose section has the shape of NACA 64A010. The aspect ratio of this hydrofoil is 6. As shown in the bottom figure, for small angle of attack there are small differences between computation and the experimental results taken from Reference 15. The differences increase as the angle of attack increases. The reason for these discrepancies may be that first, the effect of viscosity is not included in the computation, and second, the test was done with turbulence stimulation. The top figure indicates that for an angle of attack of 4 degrees, the computed lift coefficient is about twice the measured value when the submergence is large. When the ratio of submergence to chord is smaller than 0.5, the agreement between computation and experiment is good. For small submergences, the lift is more affected by the free surface than viscosity, and when the submergence is large, the reverse is true. On the other hand, compared with the experiment, the results of Wadlin and Christopher show better agreement than those by the present method when the submergence ratio is larger than 2.

When the location of the sail plane or stern plane of a submersible is at a depth of two or three times of chord, a better lift computation can be expected with the method developed in Reference 17.

Figure 16 shows forces and moment for Model 4621 with and without sternplanes at deep submergence. The computed and experimental axial forces are fairly steady at different trim angles. The vertical forces for the bare hull are computed to be significantly less than those of experiment. However, the results of vertical forces with sternplane agree very well with those of experiment except at $\alpha=12^{\circ}$. The reason for the good agreement for the case with sternplane is that the vertical force (in this case lift) of the control plane alone is over-estimated at deep submergence as shown in Figures 14 and 15; and this over-estimation is compensated with the under-estimation of the vertical forces of base hull. The moments are computed to be larger than the experimental values.

Figure 17 shows the results of vertical force of a spheroid with L/D=7 near a wall. The computed results are compared with the results of Newman.[18] Newman's method was developed using slender body theory and with the assumption of L/D >> 1 and h/D << 1. The vertical forces computed by the present method are smaller than those computed by Newman. It is unkown which method is more accurate.

CONCLUSIONS AND RECOMMENDATIONS

The forces and moment acting on a submersible moving beneath the free surface or near a wall with a pitch angle for the bare hull or a control surface deflection have been computed using potential flow theory. There is good agreement between calculation and experiment for the bare hull when the ratio of submergence depth to the diameter is larger than 1 and the pitch angle is zero. For the control planes alone, the good agreement between calculation and experiment is achieved when the ratio of submergence depth to chord is small. When this ratio is large, the force due to viscosity is dominant and the present method generally computes forces larger than those of experiment.

From the present study, the following conclusions may be drawn:

1. The numerical evaluation of the Green function needs to be improved when the ratio of submergence depth to diameter is smaller than 1.0. Near the free surface, the Green function has oscillatory behavior and the exponential function decays slowly.

2. For nonzero angle of attack, there is a cross flow or vortex shedding. The effect of cross flow or vortex shedding should be included in the computation with the help of viscous flow analysis.

3. When the ratio of submergence depth to the mean chord of a control plane is large, the lift is dominated by the contribution of viscosity. The viscous effect on the lift should be incorporated in the future computation.

4. To improve the results of potential theory, an empirical or analytical approach should be developed with inclusion of viscous effect.

ACKNOWLEDGEMENT

The author acknowledges the support of Messrs. M. Davis and D. Milne. He also expresses his thanks to Messrs. J. Feldman and T. Moran for their coordination of this work. Finally, the author thanks Mr. A. Gersten for his extensive editorial advice.

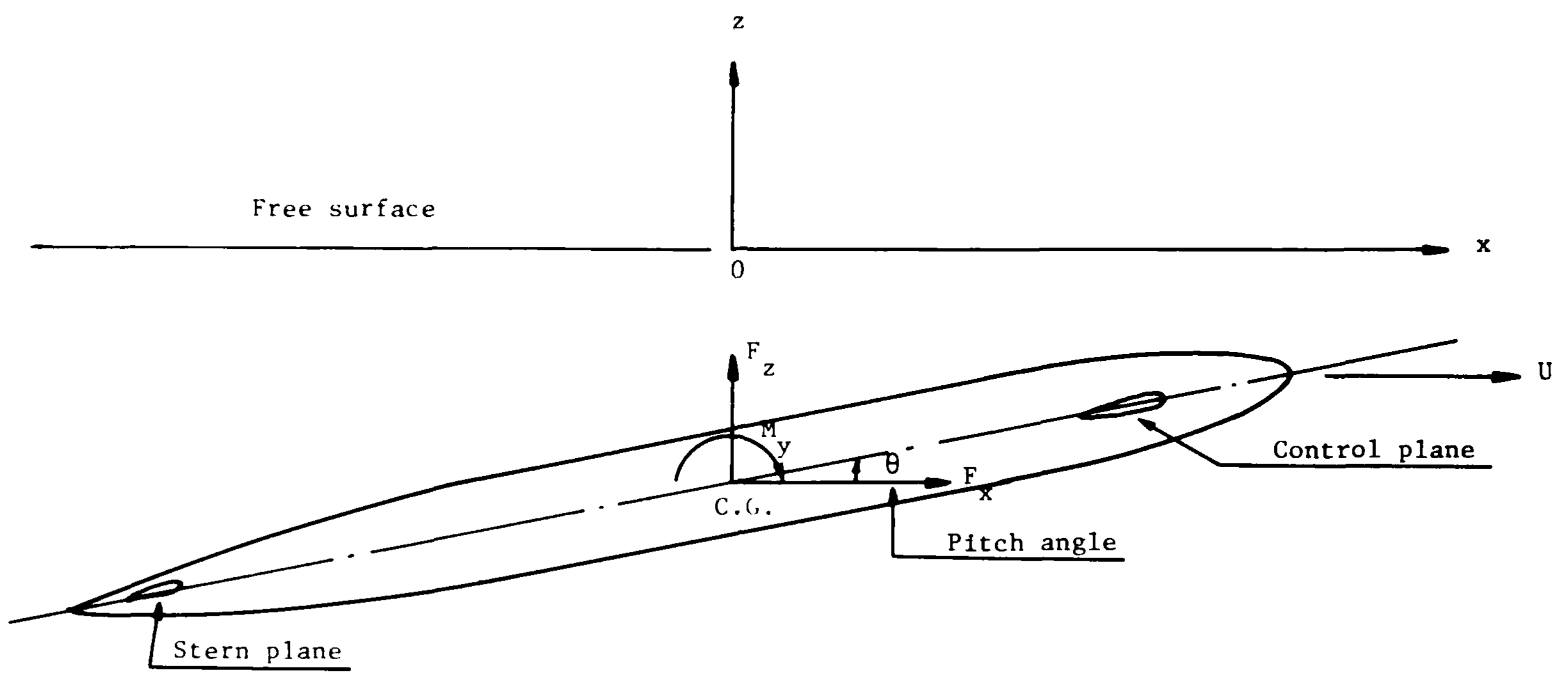

Figure 1 - Coordinate System

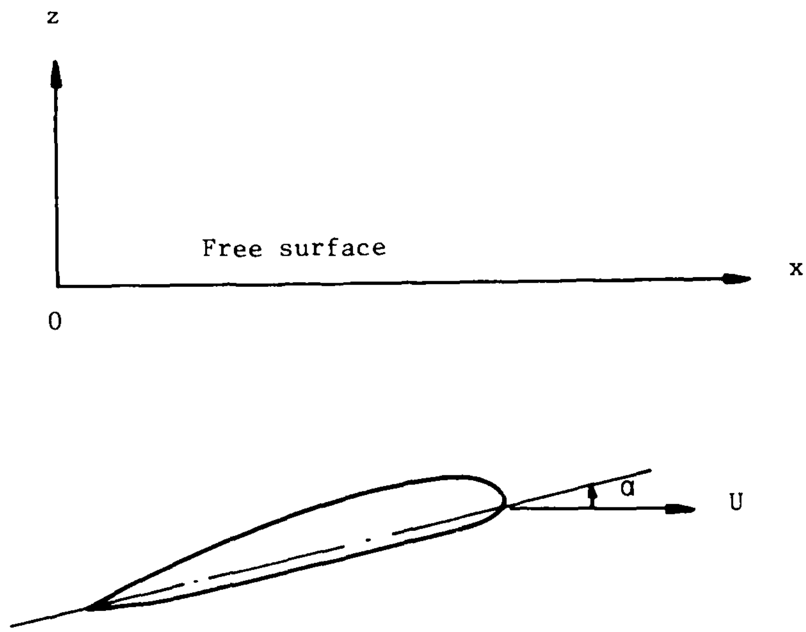

Figure 2 - Coordinate System for a Control Plane

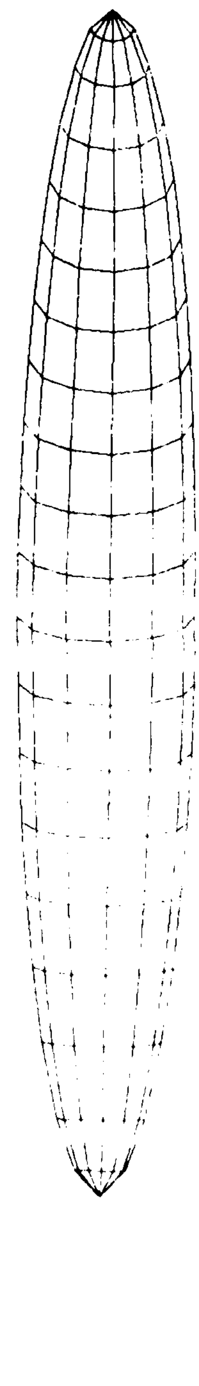

Figure 3 - Discretization of the Bare Hull

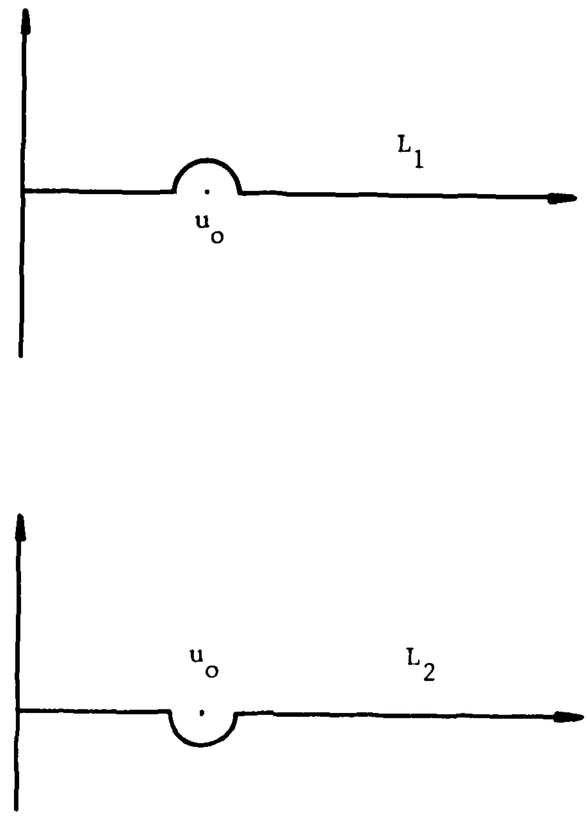

Figure 4 - Integral Paths

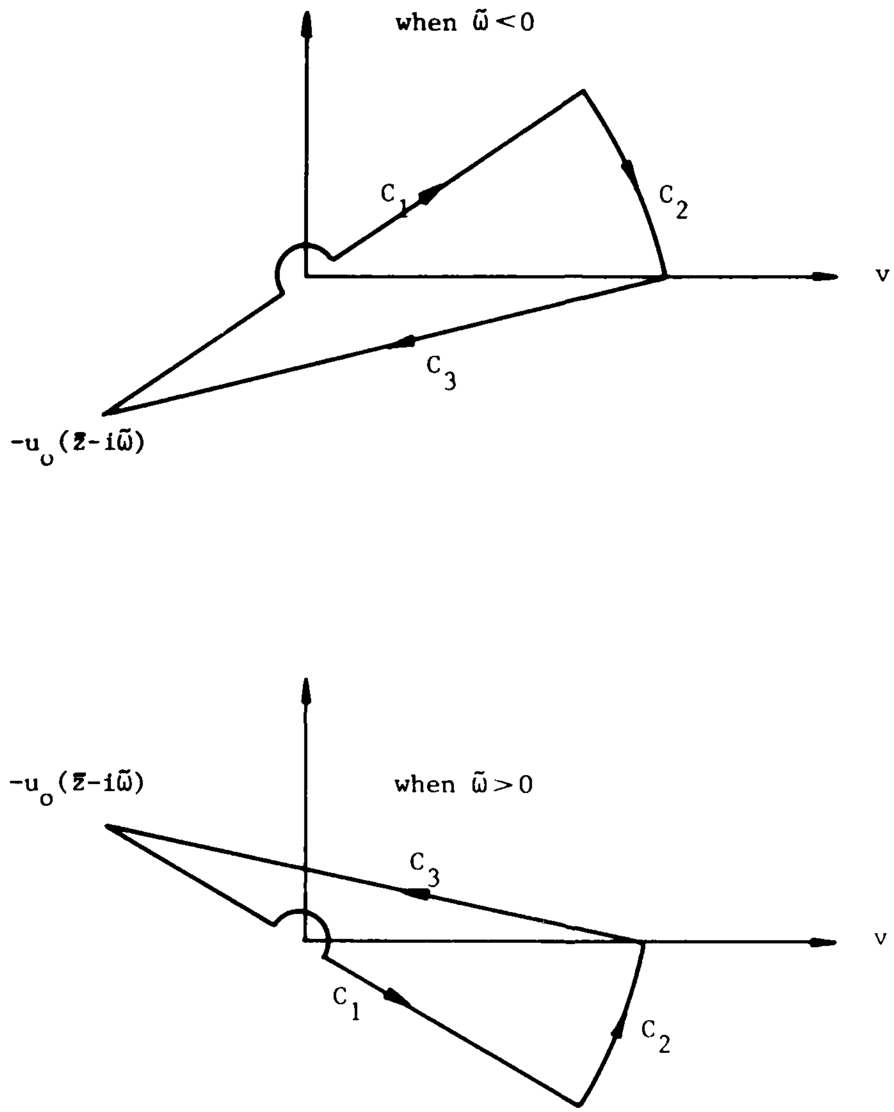

Figure 5 - Change of Integral Path for L_1

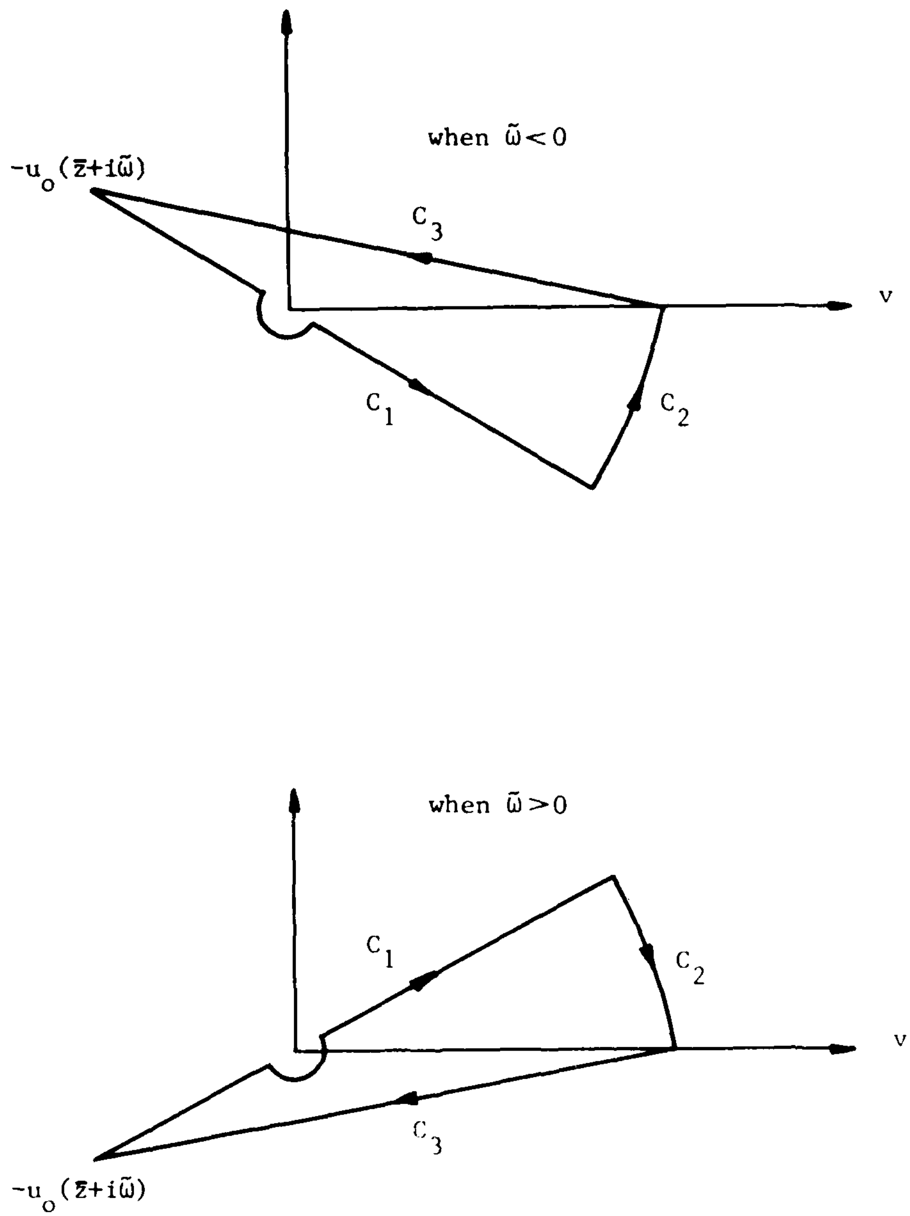

Figure 6 - Change of Integral Path for L_2

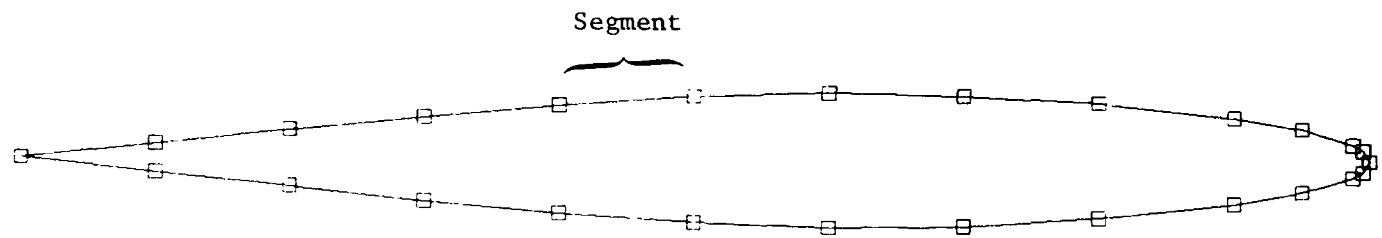

Figure 7 - Discretization of Section of a Control Plane

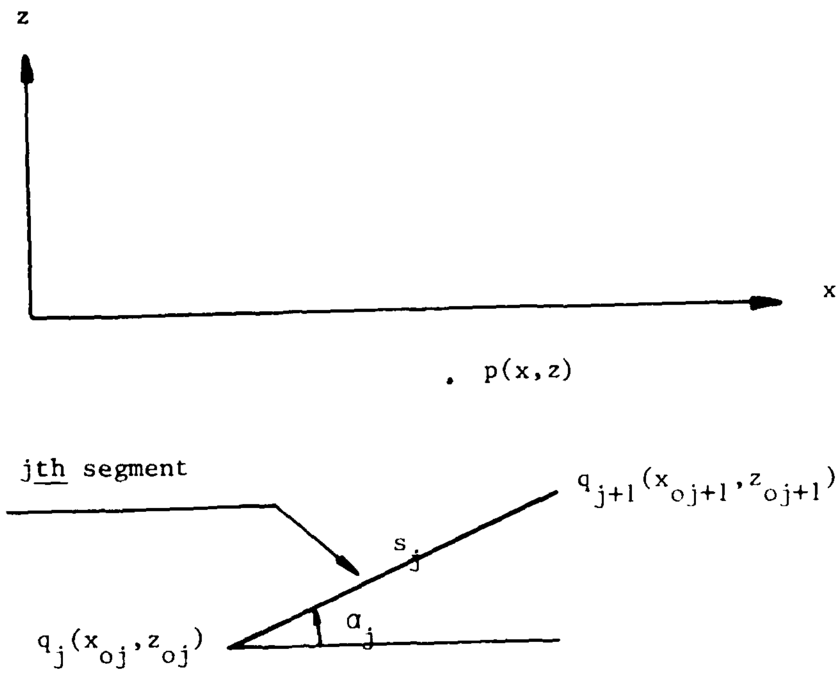

$$\alpha_j = \tan^{-1}\left(\frac{z_{oj+1}-z_{oj}}{x_{oj+1}-x_{oj}}\right)$$

$$r_j^2 = \overline{pq}_j^2 = (x-x_{oj})^2 + (z-z_{oj})^2$$

$$r_{j+1}^2 = \overline{pq}_{j+1}^2 = (x-x_{oj+1})^2 + (z-z_{oj+1})^2$$

$$\theta_j = \tan^{-1}\left(\frac{z-z_{oj}}{x-x_{oj}}\right)$$

$$\theta_{j+1} = \tan^{-1}\left(\frac{z-z_{oj+1}}{x-x_{oj+1}}\right)$$

Figure 8 - Notations for Equation (70)

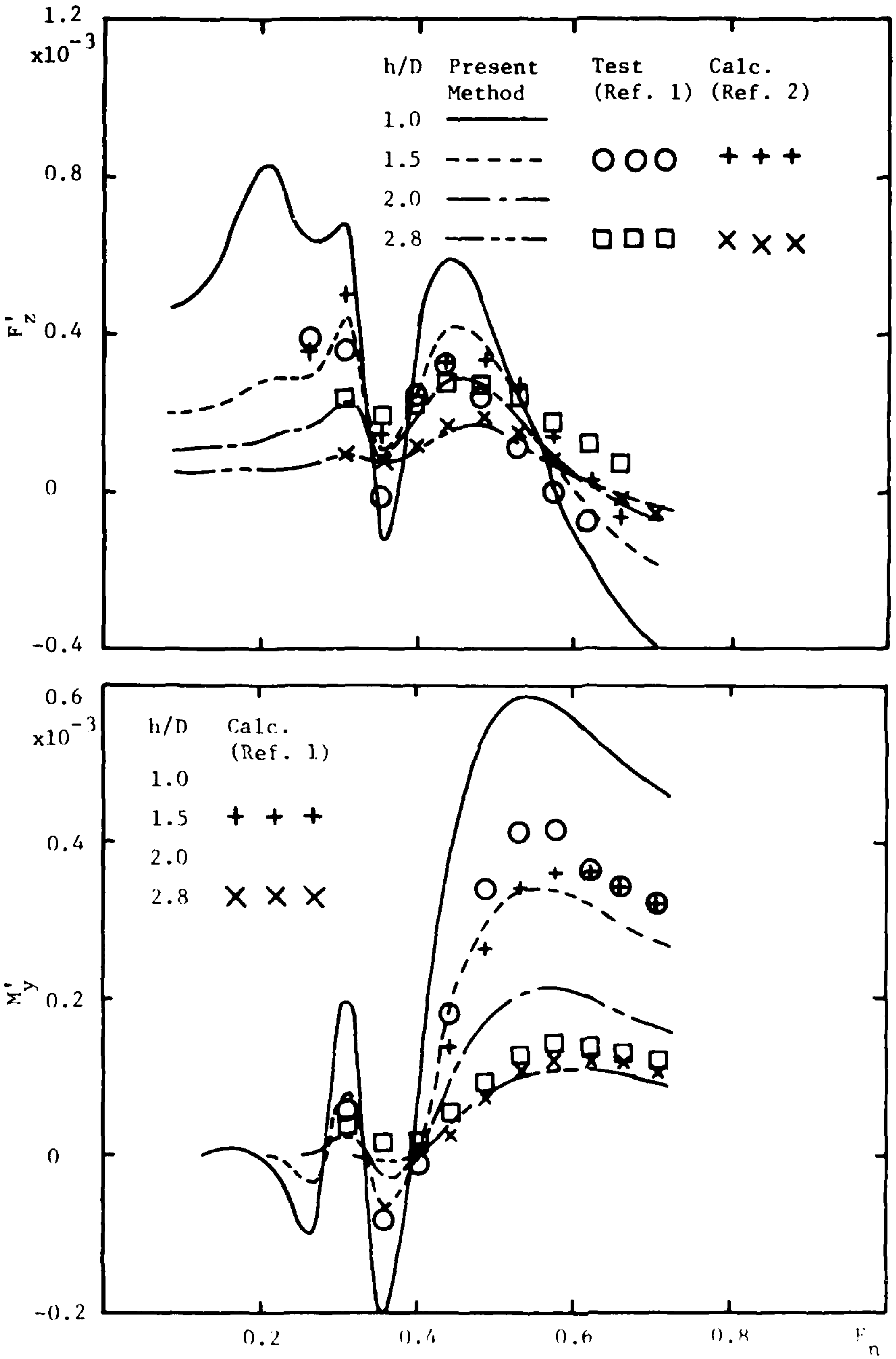

Figure 9 - Force and Moment on a Rankine Ovoid with L/D = 10.5 at Different Submergences

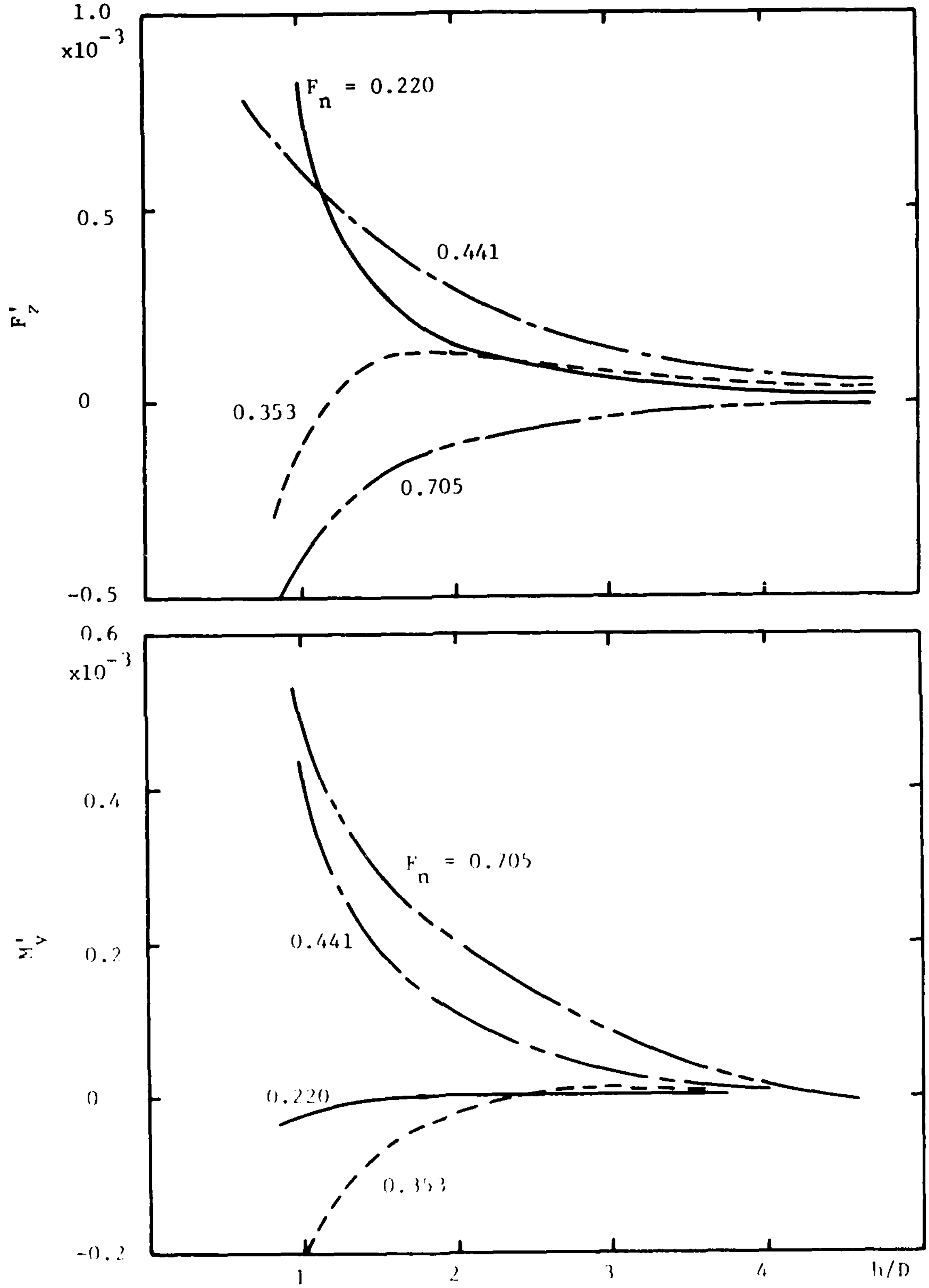

Figure 10 - Force and Moment on a Rankine Ovoid with L/D = 10.5 at Different Froude Numbers

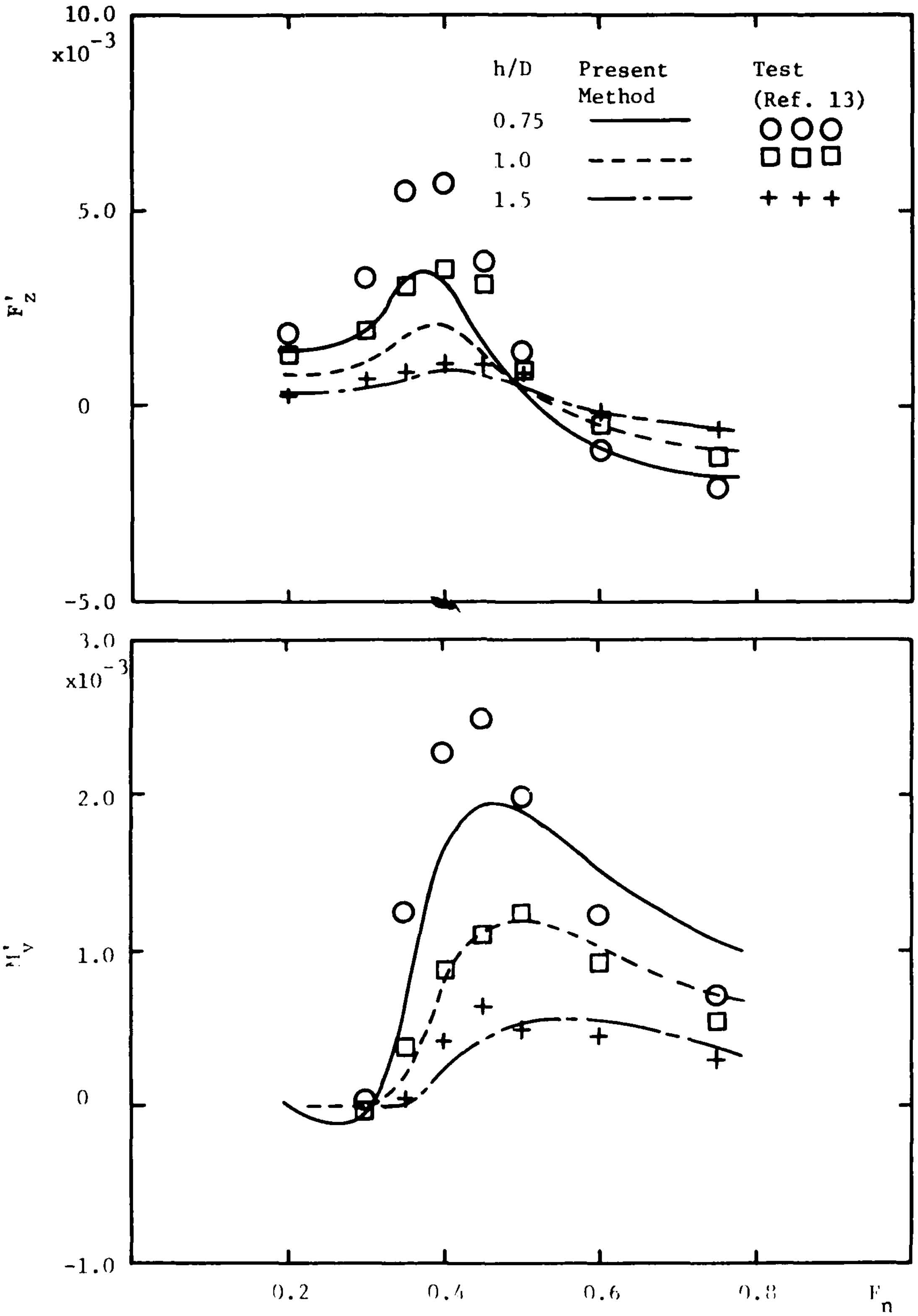

Figure 11 - Force and Moment on a Spheroid with L/D = 7 when $\theta = 0^{o}$

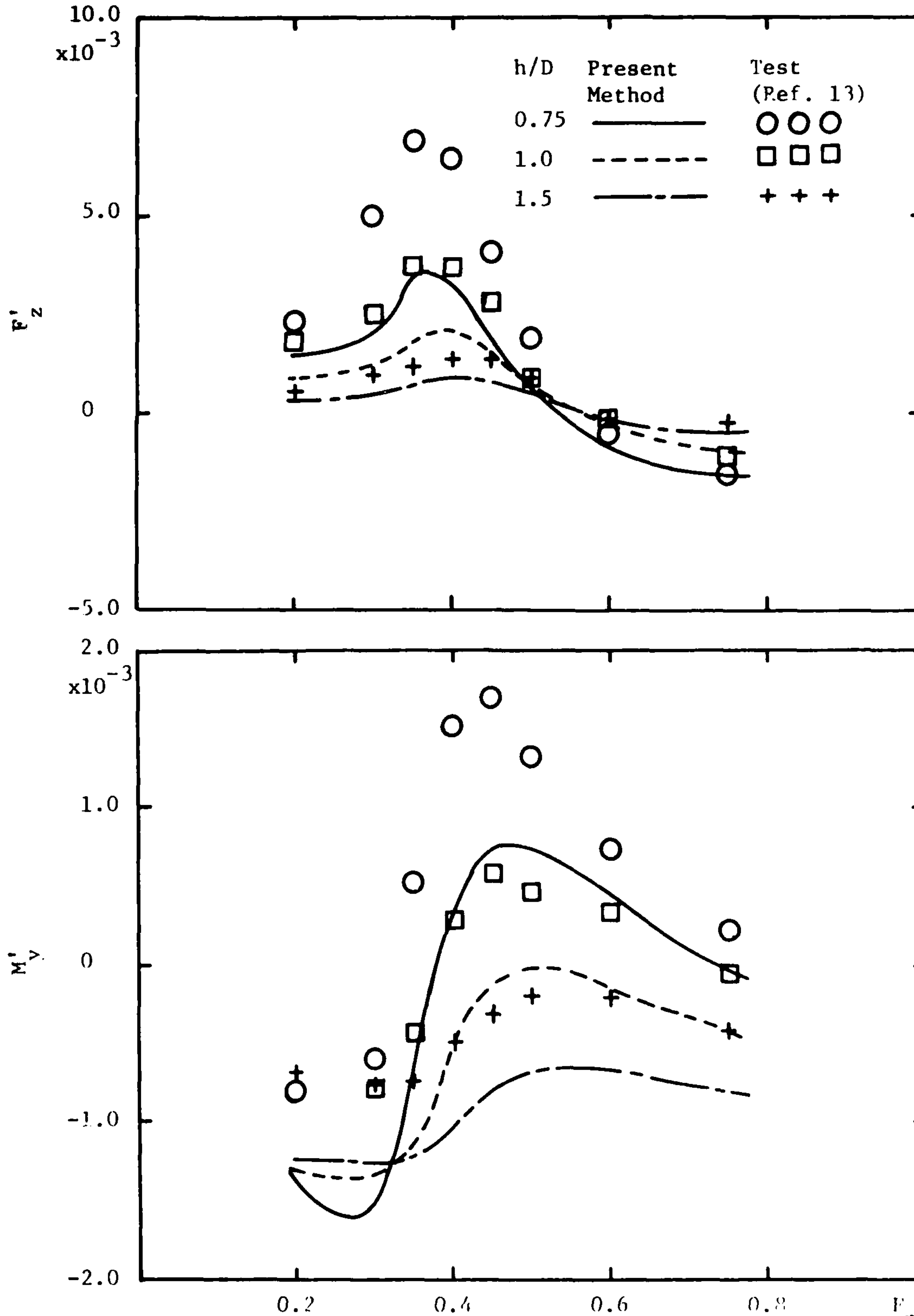

Figure 12 - Force and Moment on a Spheroid with L/D = 7 when θ = 2.5° (Bow up)

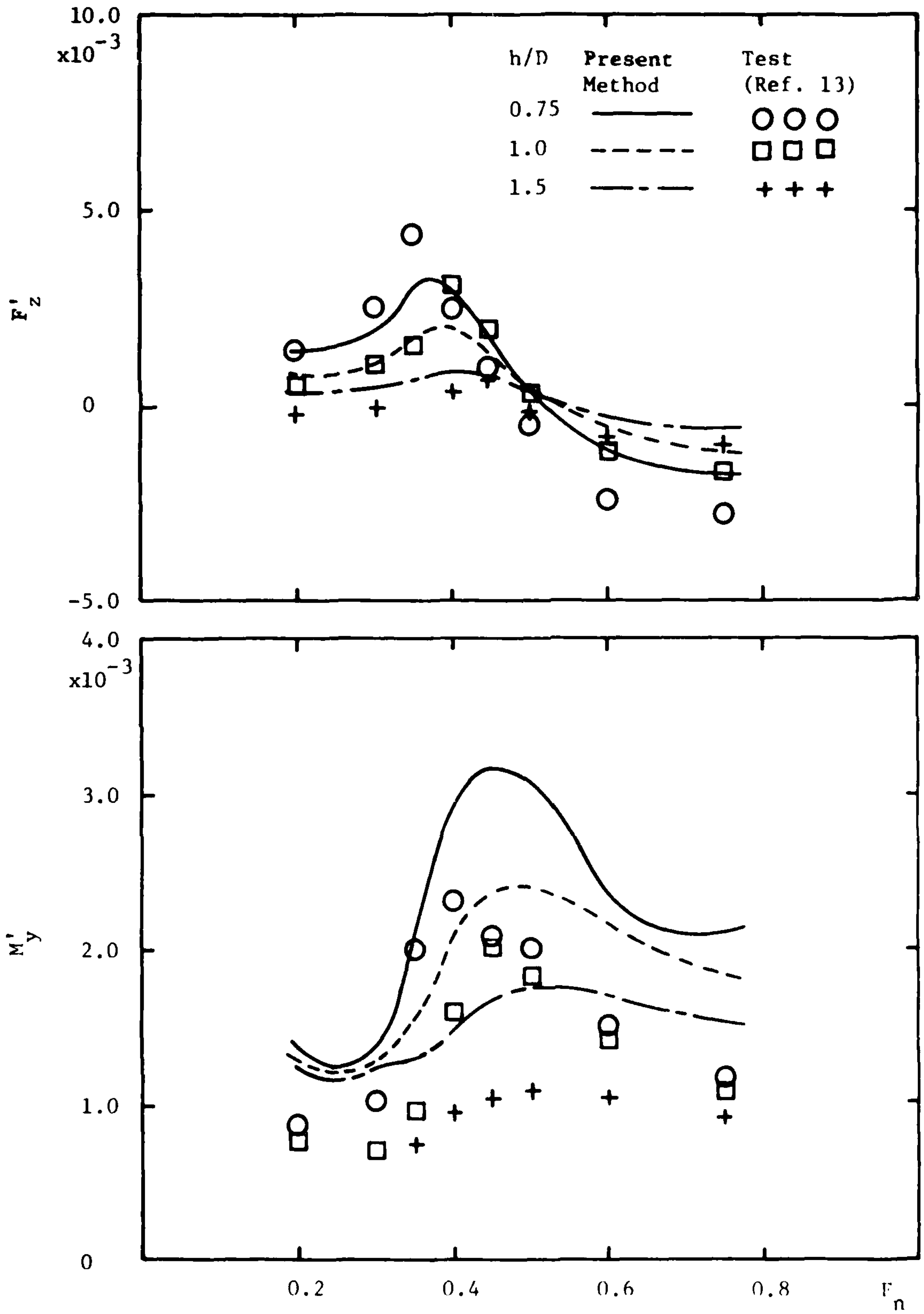

Figure 13 - Force and Moment on a Spheroid with L/D = 7 when θ = -2.5° (Bow down)

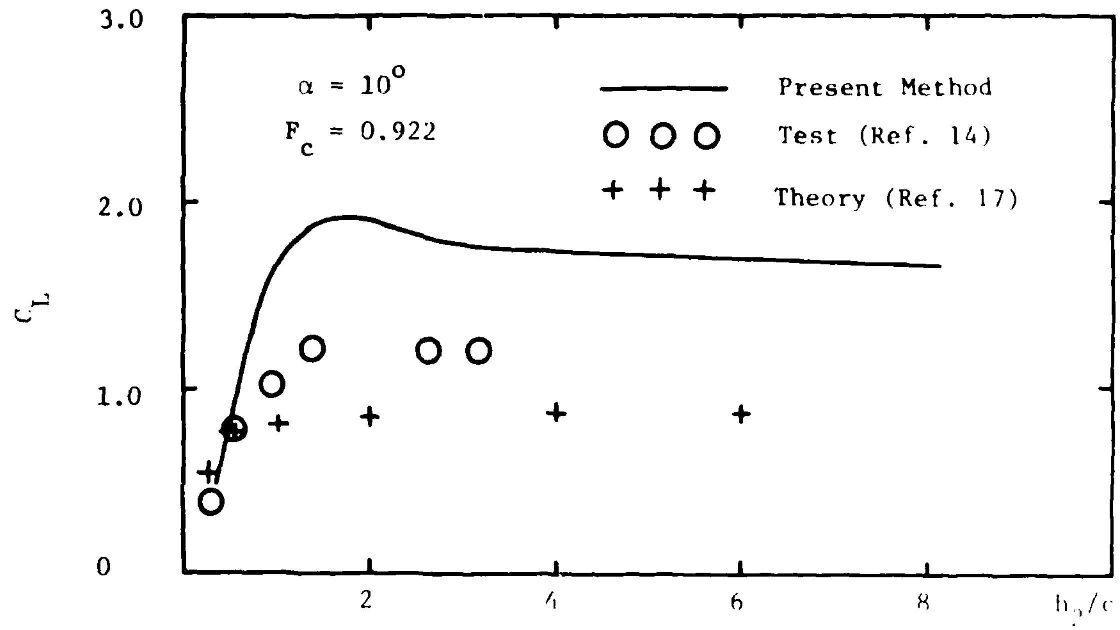

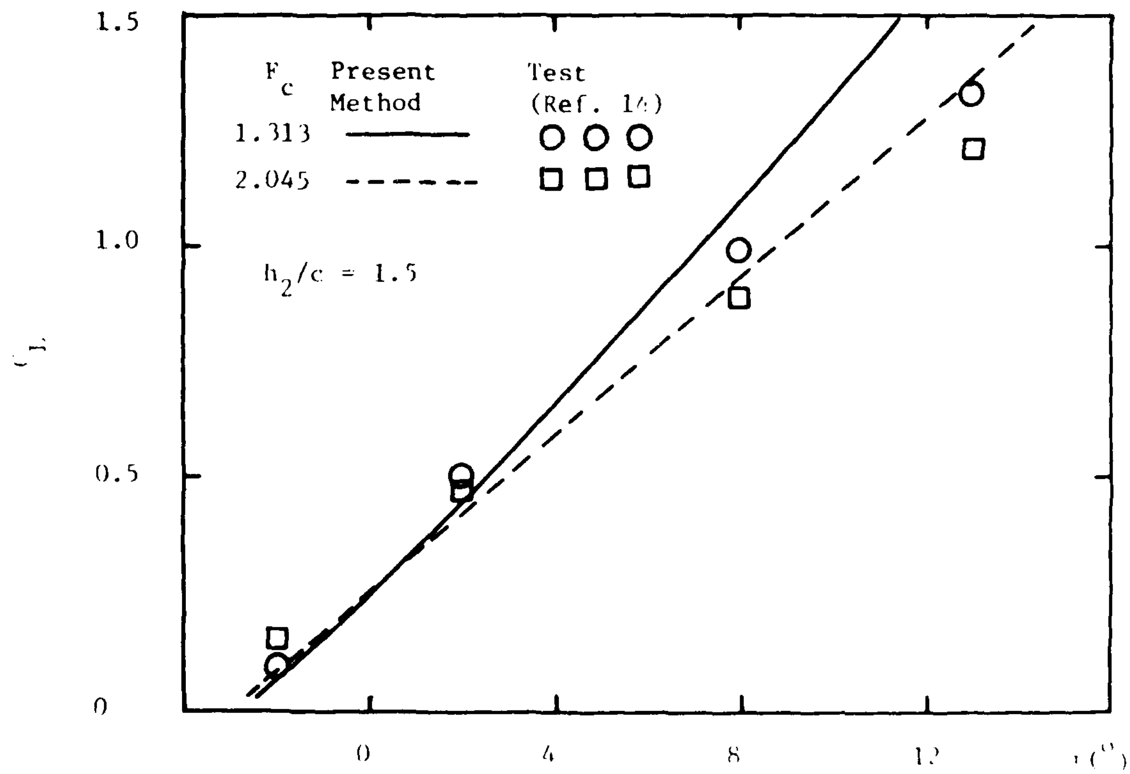

Figure 14 - Lift of a Hydrofoil of NACA 4412 Shape

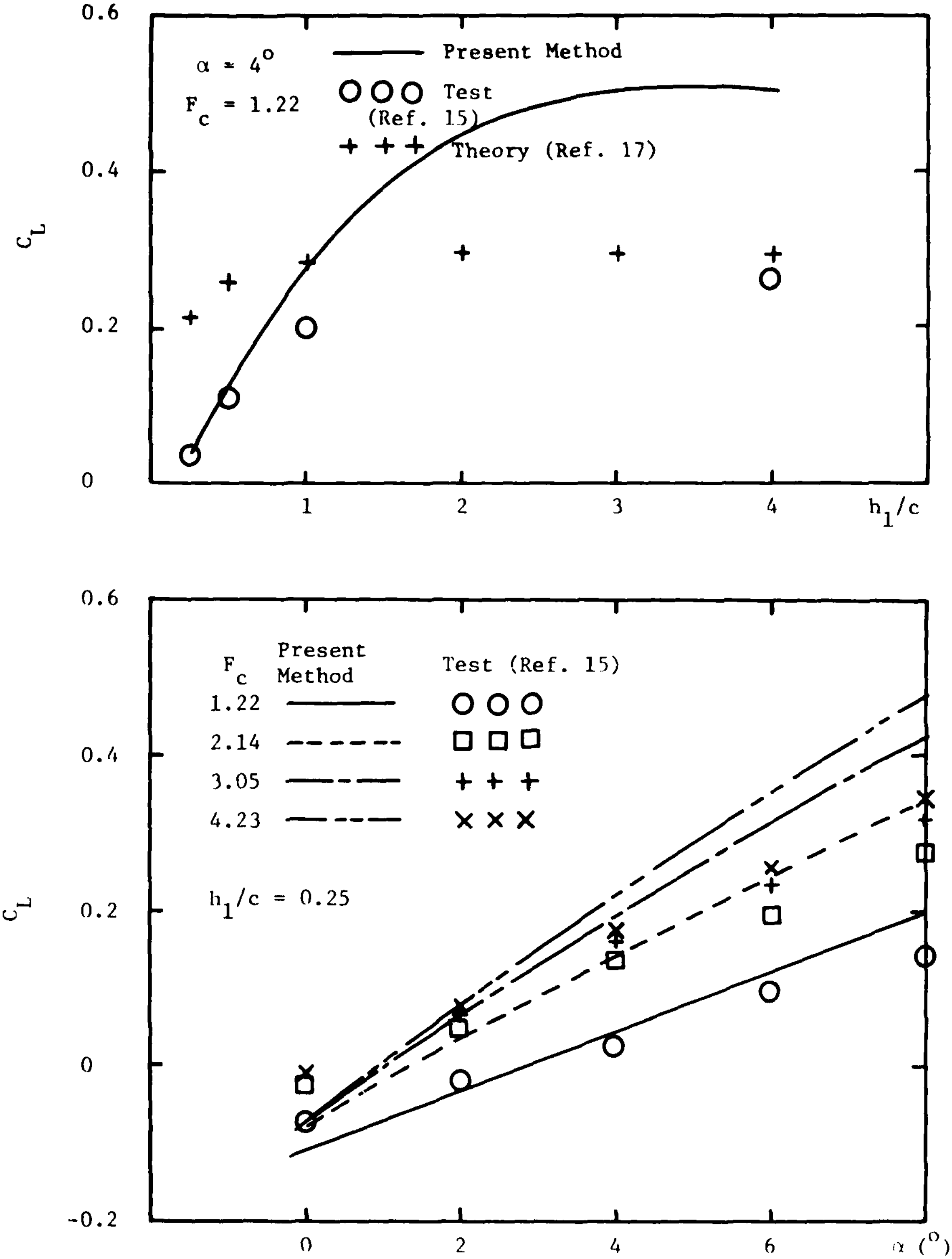

Figure 15 - Lift of a Hydrofoil of NACA 64A010 Shape

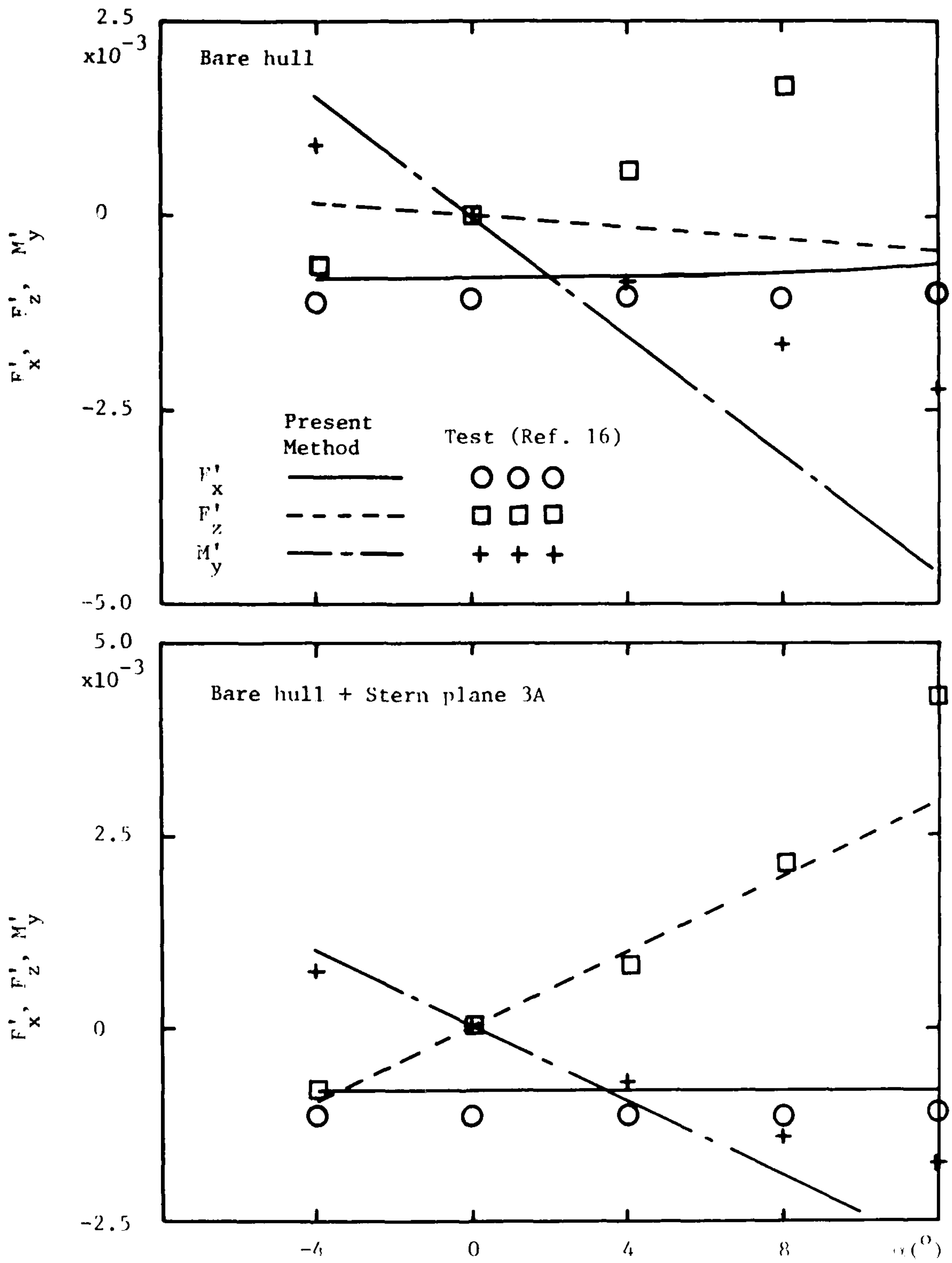

Figure 16 - Forces and Moment on Model 4621 at Deep Submergence (h/D = 4.89)

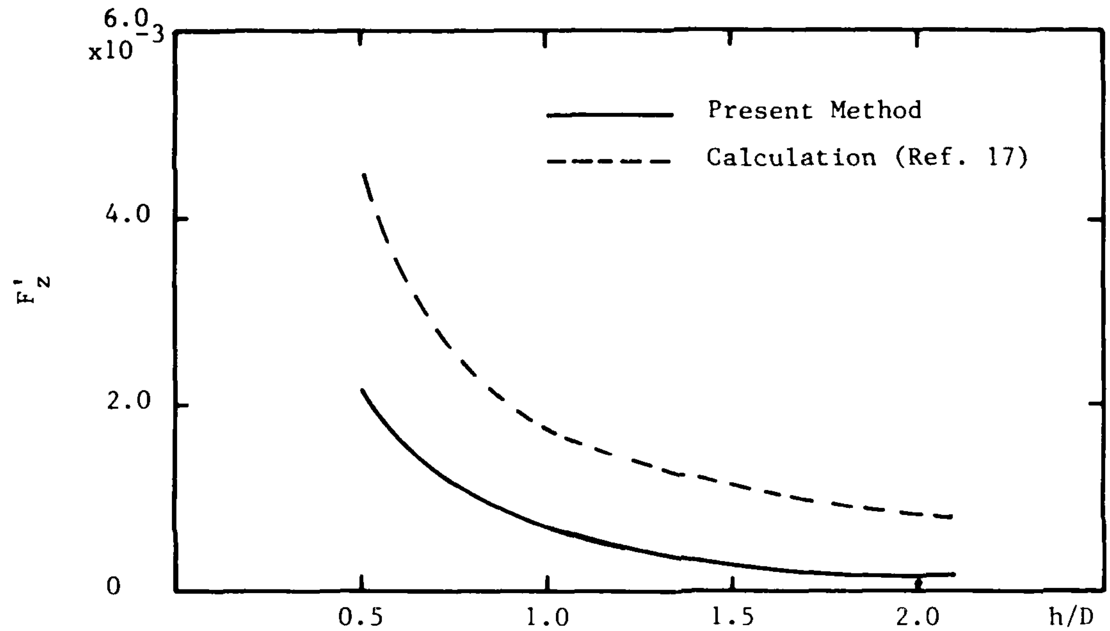

Figure 17 - Vertical Force on a Spheroid with L/D = 7 Near a Wall

REFERENCES

1. Pond, H.L., "The Moment Acting on a Rankine Ovoid Moving Under a Free Surface," Journal of Ship Research, March 1959.

2. McCreight, W.R., "Heave Force and Pitching Moment on a Submerged Body of Revolution in Finite Depth," Massachusetts Institute of Technology, Department of Naval Architecture and Marine Engineering, Report No. 70-7, June 1970.

3. Giesing, J. P. and A.M.O. Smith, "Potential Flow about Two-dimensional Hydrofoils," Journal of Fluid Mechanics, vol. 28, pp. 113-129, 1967.

4. Brard, R., "The Representation of a Given Ship Form by Singularity Distributions When the Boundary Condition on the Free Surface is Linearized," Journal of Ship Research, Vol. 16, No. 1, March 1972.

5. Wehausen, J.V. and E.V. Laitone, "Surface Waves," in Encyclopedia of Physics, vol. IX, Springer-Verlag, Berlin, 1960.

6. Milne-Thomson, L.M., "Theoretical Hydrodynamics," The McMillan Company, New York, 1960.

7. Hess, J.L. and A.M.O. Smith, "Calculation of Non-Lifting Potential Flow About Arbitrary Three-dimensional Bodies," Douglas Aircraft Co., Inc., Report No. E.S. 4062, March 1962.

8. Hong, Y.S. and J.R. Paulling, "A Procedure for the Computation of Wave- and Motion-induced Forces on Three-dimensional Bodies at Zero Forward Speed," Report to American Bureau of Shipping, May 1979.

9. Inglis, R.B. and W.G. Price, "Calculations of the Velocity Potential of a Translating, Pulsating Source," Transaction of the Royal Institution of Naval Architects, vol. 122, 1980.

10. Abramowitz, M. and I.A. Stegun, "Handbook of Mathematical Functions," Dover Publications, Inc., New York, December 1972.

11. Todd, J., "Evaluation of the Exponential Integral for Large Complex Arguments, "Journal of Research of the National Bureau of Standards, vol. 52. No. 6, June 1954.

12. Frank, W., "Oscillation of Cylinders in or below the Free Surface of Deep Fluids," David Taylor Naval Ship Research and Development Center Report No. 2375, October 1967.

13. Brooks, S.H., G. Weinblum and D.B. Young, "Forces and Moments Experienced by a Spheroid Moving Uniformly On or Near The Surface," David Taylor Naval Ship Research and Development Center Report No. 384, June 1951.

14. Nishiyama, T., "Experimental Investigation of the Effect of Submergence Depth upon the Hydrofoil Section Characteristics," Journal of Society of Naval Architects, Japan, vol. 105, 1959.

15. Wilson, M.B., "Experimental Performance of a Flapped Hydrofoil in Calm Water at Low Froude Numbers," David Taylor Naval Ship Research and Development Center Report No. DTNSRDC-82/002, June 1982.

16. Dempsey, E.M., "Static Stability Characteristics of a Systematic Series of Stern Control Surfaces on a Body of Revolution," David Taylor Naval Ship Research and Development Center Report No. 77-0085, August 1977.

17. Wadlin, K.L. and K.W. Christopher, "A Method for Calculation of Hydrodynamic Lift for Submerged and Planing Rectangular Lifting Surfaces," NACA TR R-14, 1959.

18 Newman, J.N., "The Force and Moment on a Slender Body of Revolution Moving Near a Wall," David Taylor Naval Ship Research and Development Center, Report No. 2127, December 1965.